

This document is confidential and is proprietary to the American Chemical Society and its authors. Do not copy or disclose without written permission. If you have received this item in error, notify the sender and delete all copies.

Black GaAs by Metal-Assisted Chemical Etching

Journal:	<i>ACS Applied Materials & Interfaces</i>
Manuscript ID	am-2018-10370n.R1
Manuscript Type:	Article
Date Submitted by the Author:	n/a
Complete List of Authors:	Lova, Paola; Università degli Studi di Genova, Dipartimento di Chimica e Chimica Industriale Robbiano, Valentina; Università degli studi di Pisa, Dipartimento di ingegneria dell'informazione Cacialli, Franco; University College London, London Centre for Nanotechnology and Department of Physics and Astronomy Comoretto, Davide; Università degli Studi di Genova, Chimica e Chimica Industriale Soci, Cesare; Nanyang Technological University, Physics and Applied Physics

SCHOLARONE™
Manuscripts

Black GaAs by Metal-Assisted Chemical Etching

Paola Lova,^{1,4} Valentina Robbiano,² Franco Cacialli,² Davide Comoretto³ and Cesare Soci^{1,4,*}

1 Energy Research Institute at NTU (ERI@N) and Interdisciplinary Graduate School, Nanyang Technological University, 50 Nanyang Avenue, Singapore 639798

2 Department of Physics and Astronomy and London Centre for Nanotechnology, University College London, WC1E 6BT, United Kingdom

3 Dipartimento di Chimica e Chimica Industriale, Università degli Studi di Genova, via Dodecaneso 31, 16121, Genova, Italy

4 School of Physical and Mathematical Sciences, Division of Physics and Applied Physics, Nanyang technological University, 21 Nanyang Link, Singapore 637371

KEYWORDS: Metal assisted chemical etching, anisotropic etching, perfect antireflection, black GaAs, III-V semiconductors.

ABSTRACT: Large area surface microstructuring is commonly employed to suppress light reflection and enhance light absorption in silicon photovoltaic devices, photodetectors and image sensors. To date, however, there are no simple means to control the surface roughness of III-V semiconductors by chemical processes similar to the metal assisted chemical etching of black Si. Here we demonstrate anisotropic metal assisted chemical etching of GaAs wafers exploiting the lower etching rate of the monoatomic Ga $\langle 111 \rangle$ and $\langle 311 \rangle$ planes. By studying the dependence of this process on different crystal orientations, we propose a qualitative reaction mechanism responsible for the self-limiting anisotropic etching and show that reflectance of the roughened surface of black GaAs reduces up to ~ 50 times compared to polished wafers, nearly doubling its absorption. This method provides a new, simple and scalable way to enhance light absorption and power conversion efficiency of GaAs solar cells and photodetectors.

Introduction

Scattering and antireflective superficial layers are widely used to increase photovoltaic efficiency of inorganic semiconductor,¹⁻² conjugated polymer³ and perovskite⁴⁻⁵ solar cells. Such layers relies on light trapping surfaces,⁶⁻⁷ scattering structures⁸ and photonic crystals,⁹⁻¹¹ which increase the light path within the photoactive layer, enhance light absorption, and broaden the absorption spectrum.¹² The fabrication

of these structures is often accomplished by lithographic techniques, which are hard to implement within the workflow of solar cell production. Wet processes for large area antireflection or light trapping surfaces are a low-cost, easily scalable alternative to lithography. For example, metal-assisted chemical etching (MACE) is widely used to fabricate high aspect ratio nanowire array with near-zero surface reflectivity on silicon¹³⁻²¹ and germanium²² surfaces. MACE relies on the dissolution of a substrate operated by a mixture of oxidizing and acidic or alkaline species.^{19, 23-24} In such processes, a transition metal^{13, 16, 25} catalyses the anisotropic and directional etching of the substrate surface.^{24,32,41} As a result, when the catalyst is randomly dispersed on the surface, the process generates nano- and micro-structured arrays^{14, 18, 26-27} (see Supporting Information Fig. S1 for process details). So far, only few attempts were made to extend wet etching processes to structure the surface of III-V semiconductors. MACE of GaAs was demonstrated in conjunction with thermal evaporation²⁸, or lithographic patterning of the metal catalyst²⁹⁻⁴¹ by photolithography,¹⁶ nanoimprint lithography,⁴² and microsphere self-assembly,⁴³ while the use of catalyst nanoparticles was shown using Au films evaporated on the GaAs surface and subsequently treated at high temperature.³⁹ Thermal treatment can induce arsenic vacancies⁴⁴ and lead to catalyst diffusion on the GaAs surface. So far, lithographic patterning and thermal evaporation have always been necessary to achieve the desired anisotropic etching of III-V semiconductors, substantially limiting the scalability of the process. Here we demonstrate a lithography-free MACE process for structuring GaAs surfaces with near-zero reflection⁴⁵ (*black GaAs*). The method relies on the electroless deposition of randomly dispersed gold nanoparticles cast from solution on the GaAs surface and etching in H_2O_2 and HF, which are entirely performed at ambient conditions. We find that the antireflective properties of *black GaAs* outperform those of the well-known micro-/nano-structured silicon (*black Si*), yielding reflectance values as low as 0.013.

Experimental Methods

Metal-assisted chemical etching: MACE was performed on silicon doped *n*-type (111)B, (100), (211) and (110) GaAs epi-ready wafers (purchased from Axt Inc). In a typical process, gold nanoparticles are deposited on the semiconductor surface by immersion in a water solution containing 0.1 mM of AuCl_3 . Samples are then blow dried and etched in HF: H_2O_2 (4:1) for 10 minutes.

Reference *black Si* samples were fabricated by a standard two-step process of *p*-type (100) Si wafers (purchased from Lotech Scientific). First, samples are etched in a solution of H_2O_2 :HF (9:1) containing 0.02 M of AgNO_3 for one hour. Then, further etching in H_2O_2 and NH_4OH (1:3) is used to remove residual catalyst and etching by-products from the surface (see Supporting Fig. S6).

Structural and optical characterization: Microstructure and topography images of the etched surfaces were obtained by scanning electron microscopy (SEM). Data were collected by a field emission SEM Jeol JSM-6700F using acceleration voltage of 5.0 kV and using high (SEI) and low (LEI) secondary electrons detectors. Individual SEM images were analysed to extract surface features sizes and orientations. Representations of the GaAs crystal lattice were elaborated with the software VESTA⁴⁶ using data retrieved from the Crystallography Open Database.⁴⁷

Reflectance was measured with a spectrophotometer (Andor Shamrock 163i) equipped with an integrating sphere (Bentham IS4-ODM-X) in the spectral range between 550 and 1100 nm. In the 1200-2600 nm spectral range, data were acquired in a fibre-based optical setup with a Micropak DH2000BAL light source and an Arcoptics FT-interferometer (1000–2600 nm, resolution 8 cm⁻¹).

Photoluminescence external quantum efficiency was measured as previously reported by the method reported by De Mello *et al.*,⁴⁸⁻⁵⁰ using an integrating sphere (Avantes AvaSphere-50) coupled to a CCD spectrometer (Avantes 2048) in the 200–1100 nm spectral range. The excitation source was a red diode laser (CNI model MRL-655) with 400 mW power. Wavelength dependent photoluminescence measurements were performed with a spectrofluorometer (Horiba Fluorolog) equipped with a Si CCD detector. The excitation source was a Xe discharge lamp.

Results and Discussion

We developed a two-step etching process of GaAs wafers via the electroless deposition of metal nanoparticles (etching catalyst) followed by etching in an acidic oxidizing bath. Randomly dispersed Au nanoparticles are precipitated from an AuCl₃ water solution on the GaAs surface by redox reaction between the Au³⁺ ions, which are reduced to Au⁰, and GaAs, which is oxidized (see Supporting Information Fig. S2). The substrate is then immersed in a bath containing H₂O₂ and HF for 10 minutes to initiate the catalytic process. Figs. 1a and 1b show the scanning electron micrographs of etched GaAs surfaces with crystallographic orientation (111)B. The topographic images (left side) show the morphology of surface features, while the compositional images (right side) highlight the presence of residual gold nanoparticles, which are also visible as brighter spots in topographic images.

Etching of the (111)B surface produces randomly oriented, faceted hillocks with heights of about 5.5 μm and width of about 5 μm. It can be immediately noticed that the microfacet orientation remains constant throughout the sample surface, indicating a crystal plane dependent etching rate. This is further confirmed by the SEM micrographs of etched wafers with crystal orientations (100), (211) and (110) (see Supporting Information Fig. S3 and Fig. 1d).

Slow etch rate planes can be identified with the microfacet orientations comparing them with a representation of the GaAs crystal structure (Figs. 1c and 1f). Fig. 1c shows that the side facets of the hill-ocks protruding from the (111)B surface form angles of 70° (blue dotted lines) or 79° (green dashed lines) with the latter, corresponding to the $(\bar{1}31)$ and $(\bar{1}\bar{1}1)$ crystallographic orientations. Similarly, the angle between the facets (blue dotted lines in Fig. 1f) and the (100) plane (orange lines in Fig. 1f) have an angle of 26° with respect to the (100) plane, corresponding to slow etch rate planes $(3\bar{1}\bar{1})$ and $(\bar{1}\bar{1}\bar{1})$.

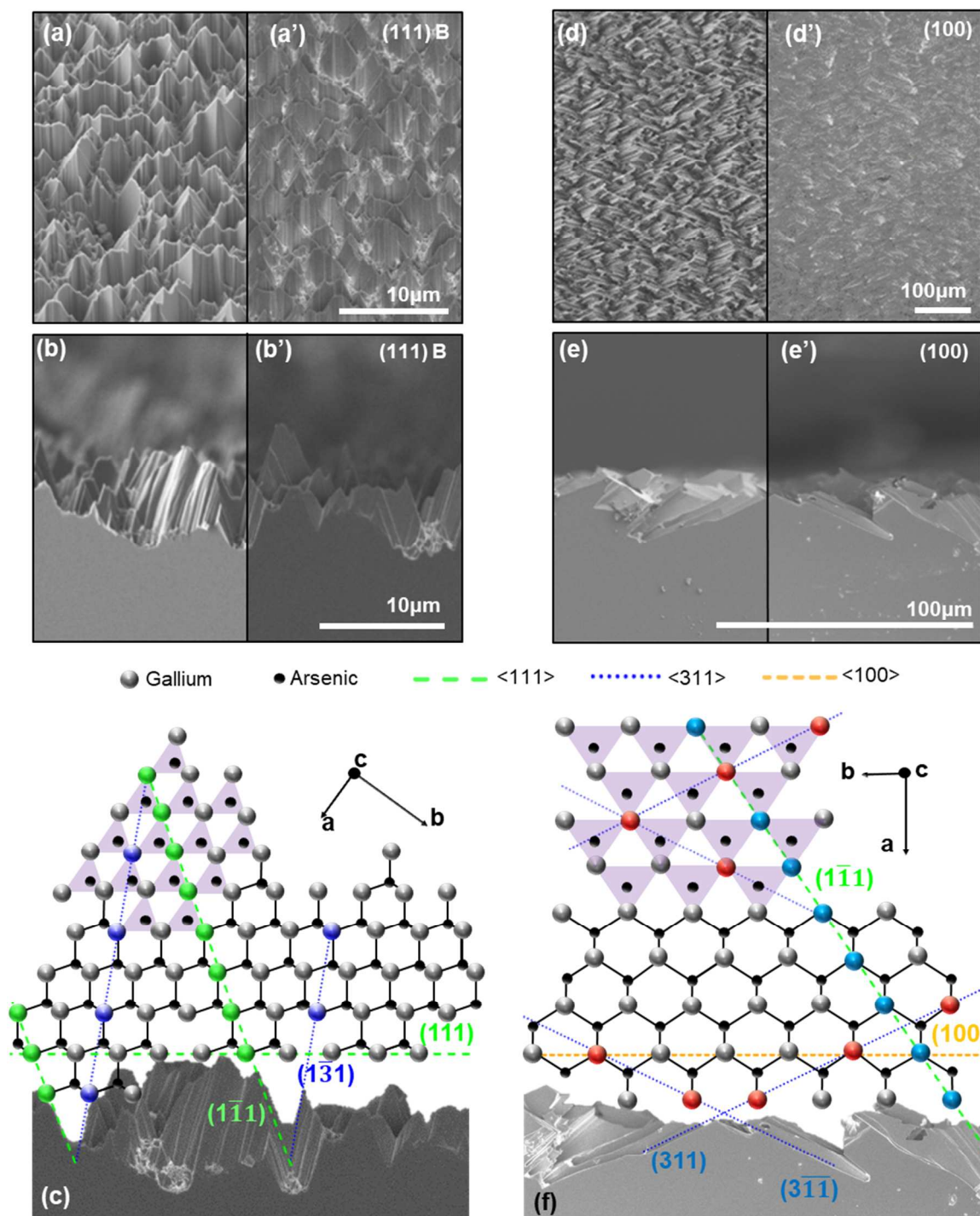
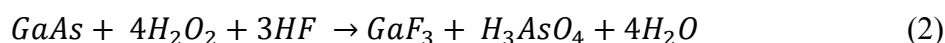
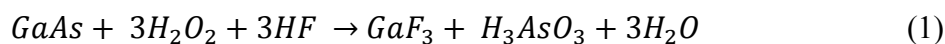


Figure 1: SEM imaging and analysis of the etched (111)B (panels a-c) and (100) (panels d-f) surfaces of GaAs. Top: tilted (a,a' and d,d') and cross-sectional views (b,b' and e,e') in topographical (a-d) and compositional (a'-d') modes. Bottom: GaAs crystal representations overlaid to the etched surface profiles (c and f).

The fact that monoatomic $\langle 111 \rangle$ and $\langle 311 \rangle$ planes are etched at slower rate than others can be understood considering the reactivity of individual Ga and As atoms. The sp_3 hybridization of Ga and As atoms in the zinc-blende crystallographic structure of GaAs stabilizes gallium, which is normally trivalent, and destabilizes arsenic, which has preferential valence five in electrophilic environment. Since the presence of a lone pair of electrons in As atoms allows their oxidation, a plausible etching mechanism would involve the oxidation of As^{3-} to As^{3+} and As^{5+} to produce arsenous and arsenic acids, while fluoride ions withdraw the gallium ions, accordingly to the following reactions:



The reactivity of Ga and As is also linked to the number of bonds that they form with the underlying crystal.⁵¹ When reactive arsenic is etched away from the (111) plane, it reveals a layer of gallium atoms singularly bounded to the crystal, which can be complexed by the fluorine ions. On the other hand, Ga atoms laying on $(1\bar{1}1)$ and $(1\bar{3}1)$ surfaces have respectively two and three bonds with the crystal and are therefore less reactive, slowing down the etch rate (see Supporting Information Fig. S4).

Fig. 2 shows a schematic of the proposed etching mechanism that accounts for the different reactivity of the species involved. Here, a gold nanoparticle laying on the GaAs (111)B surface is oxidized in an acidic environment by H_2O_2 to form gold ions (1).⁵² The resulting Au^{3+} and Au^{1+} ions diffuse along the surface until they encounter a reactive arsenic site and selectively oxidize it producing Au^0 and arsenous and arsenic acids (2). While the newly precipitated gold is subsequently reduced by H_2O_2 and becomes available for the oxidation of another reactive site, gallium atoms belonging to the (111)A plane can be complexed by the fluorine ions, thus allowing diffusion of the metal catalyst to the inner surface (3). The process continues until the $\langle 111 \rangle$ and $\langle 311 \rangle$ monoatomic gallium planes are exposed at the surface (4, 5). To confirm this mechanism, a (111)B GaAs surface was etched without catalyst. In this case, no structure attributable to a plane dependent etch rate is discernible on the resulting surface (see Supporting Information Fig. S5). Note that previous works that made use of continuous metal film as etching catalyst^{33-35, 53} could not identify the crystal plane dependent etching mechanism since gold diffusion to the active sites is inhibited by the catalyst film itself.^{32, 54}

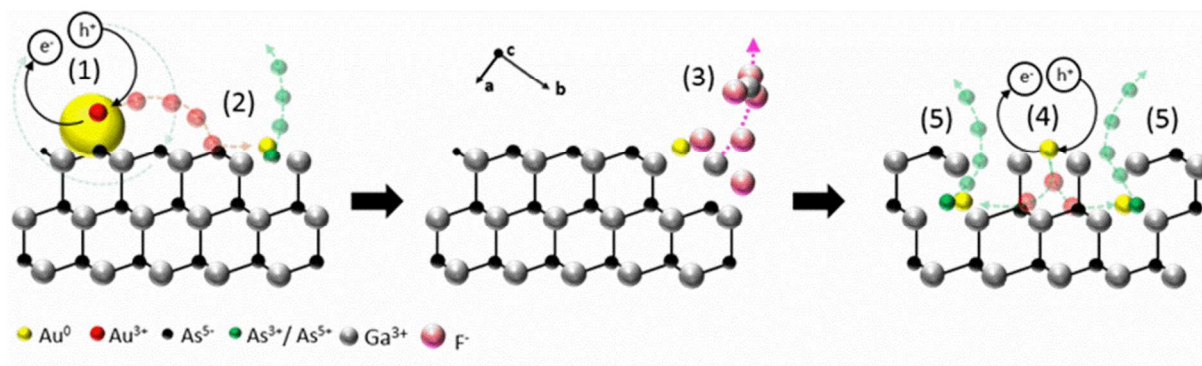


Figure 2: Schematic of the etching process of a (111)B GaAs plane assisted by a gold nanoparticle. (1) Oxidation of the Au nanoparticle by H_2O_2 to form Au ions; (2) Diffusion of Au^{3+} and Au^{1+} ions and oxidation of a reactive As site to produce Au^0 and arsenous and arsenic acids (H_3AsO_3 and H_3AsO_4); (3) Reduction of precipitated Au by H_2O_2 (which becomes available for the oxidation of another reactive site), and complexation of Ga atoms in the (111)A plane by F^- ions allow diffusion of the metal catalyst to the inner surface; (4,5) Iteration of the process leads to the exposure of the $\langle 111 \rangle$ and $\langle 311 \rangle$ monoatomic gallium planes.

Etched GaAs samples appear completely black (see insets of Figs. 3c and 3d), a very desirable property for absorber layers in photovoltaic and photodetection applications. This is due to the nearly perfect suppression of reflectance by the roughened surface, very much alike *black Si* in which silicon nanowires are formed at the surface by MACE catalysed by AgNO_3 in HF and H_2O_2 (see Experimental Section and Supporting Information Fig. S6). Fig. 3a compares the antireflective properties of *black GaAs* to those of a reference *black Si* sample. Compared to polished Si surfaces with reflectance between 0.62 and 0.90 in the range of 550 to 1150 nm (grey line in Fig. 3a), the reflectance of *black Si* oscillates from a minimum of ~ 0.04 to a maximum of ~ 0.2 , corresponding to a ~ 3 to 20-fold reduction. The low surface reflectance of *black Si* is due to the low refractive index effective medium formed by the nanowire layer, which is also responsible for the pronounced spectral oscillations with typical Fabry-Perot pattern⁵⁵ (orange line in Fig. 3a). In comparison, the reflectance of *black GaAs* (black and green lines in Fig. 3a) is between ~ 25 -60 times lower than polished GaAs (red line in Fig. 3a). On average, the antireflective properties of *black GaAs* are ~ 2 to 10 times better than *black Si* (Supporting Information Fig. S7). Note that similar results were also obtained by diffuse reflectance measurements in an integrating sphere (Supporting Information Fig. S8). As shown in the following, the nearly perfect antireflection properties of *black GaAs* stem from a completely different optical mechanism than refractive index matching in *black Si*.

Fig. 3b details the specular reflectance properties of the two types of etched GaAs samples. While both samples effectively reduce the reflectance of polished GaAs (red line in Fig. 3a), both above (absorbing

region) and below the band gap at 890 nm (1.4 eV), etched GaAs (111)B has much lower reflectance than etched GaAs (100). The lack of an interference pattern in the spectra of etched GaAs samples suggests that suppression of reflectance is due to light scattering from the micro-structured surface rather than to refractive index matching by a surface effective medium like in the case of *black Si* (See Supporting Information Fig. S6). To further confirm this hypothesis, we plotted the reflectance collected at 800 nm as a function of the inclination angle of the faceted surface of the three samples (inset of Fig. 3b). The reflectance of the polished surface (0°) is the highest, and decreases exponentially with the inclination angle of the facets on the etched surfaces (26° for the (100) and 79° for the (111)B surface, see also Fig. 1). This shows that geometrical light trapping induced by the specific geometry of the surface microfacets of *black GaAs* is the primary reflection suppression mechanism. Fig. 3c compares the near-infrared reflectance of polished and etched (111)B GaAs surfaces. While polished GaAs is highly reflective and spectrally flat throughout the entire near-infrared range (red line), the reflectance of etched GaAs varies between 0.08 at 1200 nm and 0.05 at 2600 nm (black line), corresponding to a 100 fold decrease compared to the polished surface. This makes black GaAs very interesting also for near-infrared photodetector applications.

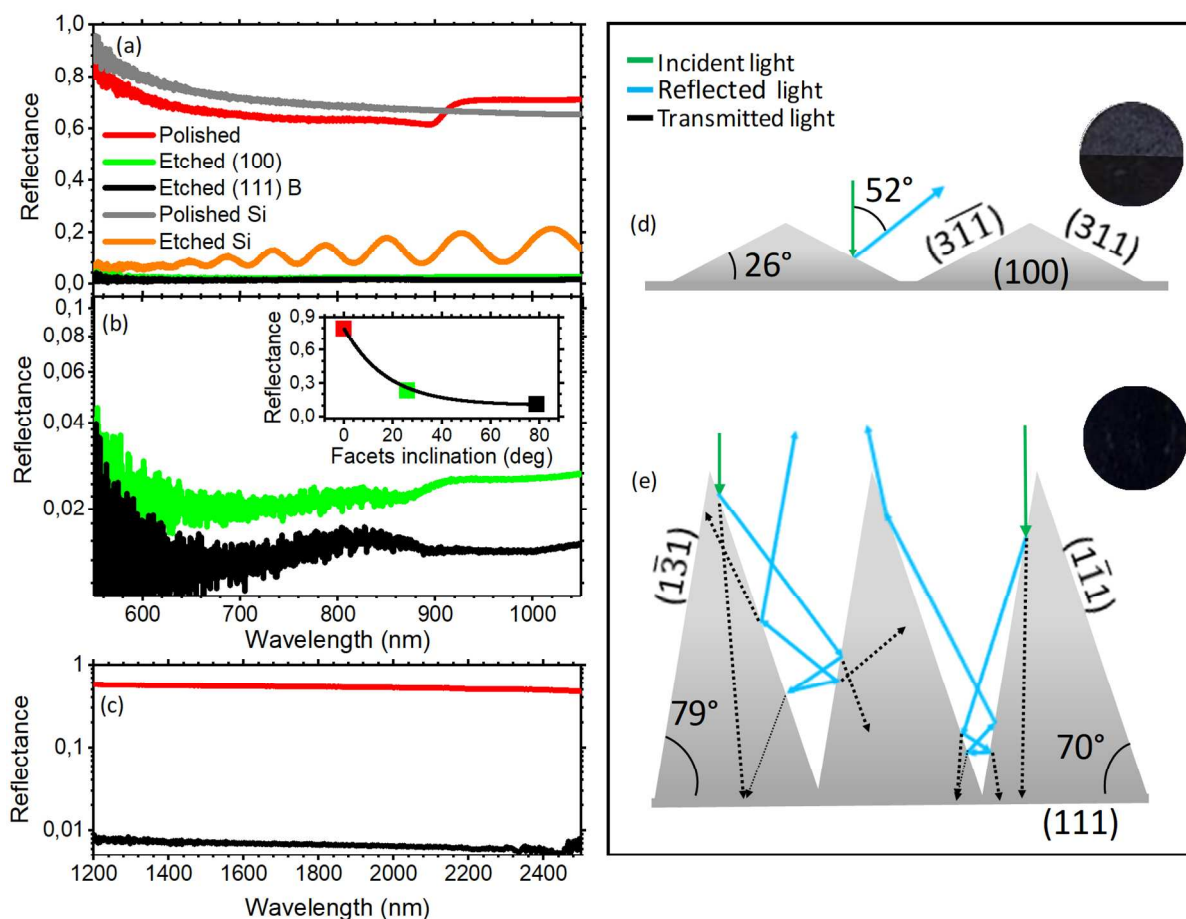


Figure 3: a) Normal incidence reflectance of polished (red line) and etched (100) (green lines) and (111)B (black lines) GaAs surfaces and of polished (grey line) and etched (orange line) Si surfaces. b) Magnified view of the reflectance spectra of the two GaAs etched surfaces. The inset shows the experimental (squares) and fitted (black line) dependence of the GaAs reflectance collected at 800 nm on the angle of inclination of the faceted surface. c) Normal incidence reflectance of polished (red line) and etched (111)B (black lines) GaAs surfaces in the near infrared spectral region. d, e) Geometrical ray-tracing analysis of the light path within ideal (100) (c) and (111)B (d) micro-faceted surfaces. The insets of c and d show the overlaid photograph of the etched wafers taken at different collection angles.

A simple ray-tracing analysis of the incident light path within the (111)B and (100) etched surfaces provides a qualitative explanation of the light trapping process (Figs. 3d and 3e). Fig. 3d shows an ideal representation of the $(1\bar{1}1)$, $(1\bar{3}1)$ and (111) facets on the etched (111)B surface (refer to Fig. 1c), while Fig. 3e depicts the $(3\bar{1}1)$ and (311) facets on the (100) etched surface (refer to Fig. 1f). The microfacets on (100) etched surfaces reflect normal incident light at $\sim 52^\circ$, resulting in strong light scattering and minimal light trapping. Conversely, the $(1\bar{1}1)$ and $(1\bar{3}1)$ microfacets on (111)B etched surfaces redirect specularly reflected normal incidence beams toward the bottom of the valleys between facets, which undergo multiple reflections before leaving the surface. Therefore, the larger inclination of surface microfacets explains the superior antireflective characteristics of etched GaAs (111)B compared to (100).

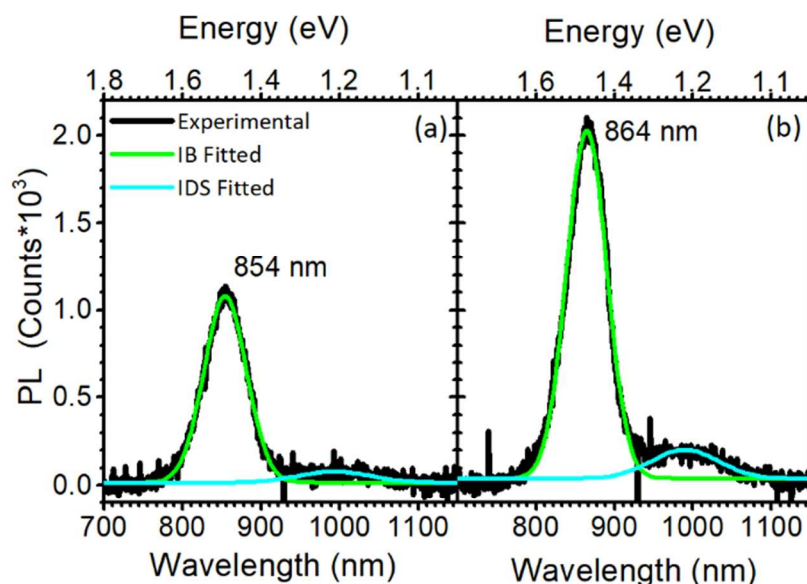


Figure 4: Photoluminescence emission spectra of a) polished and b) etched (111)B GaAs samples (black lines). The green and cyan lines are Gaussian fits to the data corresponding to conduction to valence band (CV) transitions and intra-gap transitions from defect states (IDS), respectively.

Last, photoluminescence spectra and quantum yield measurements were used to gauge the effectiveness of light trapping in *black GaAs*. Fig. 4 compares the emission spectra of polished GaAs (Fig. 4a) and

etched GaAs (111)B (Fig. 4b) under 559 nm excitation. Both samples show two emission peaks in the near infrared range, below the band gap. The most intense peak (at 853 and 864 nm in polished and etched GaAs, respectively) is due to the conduction to valence band interband transition (CV),⁵⁶⁻⁵⁷ while the weaker peak (1010 nm in both samples) is assigned to transitions from intragap defect states (IDS), commonly generated from silicon n-type doping.⁵⁶⁻⁵⁷ The 13 nm (~24 meV) shift of the CV peak and the enhancement of the IDS emission may be ascribed to the formation of new species (e.g. Ga₂O₂ and As₂O₃) on the etched surface, or to the formation of defects and increase of porosity, which are known to cause strain and lattice distortion.⁵⁸

Table 1: Absorption (Abs) at 559 nm and total (η_{tot}), interband transition (η_{CV}) and intraband surface defect state transition (η_{IDS}) photoluminescence external quantum efficiency of polished and etched (111)B GaAs.

	Abs ($\lambda_{\text{ex}}=559 \text{ nm}$)	η_{tot} (%)	η_{CV} (%)	η_{IDS} (%)
Etched	0.9	$3.6 \cdot 10^{-2}$	$2.6 \cdot 10^{-2}$	$1.0 \cdot 10^{-2}$
Polished	0.5	$3.6 \cdot 10^{-2}$	$3.2 \cdot 10^{-2}$	$0.4 \cdot 10^{-2}$
Ratio (Etched/Polished)	1.8	1.0	0.8	2.5

Notably, the photoluminescence intensity of *black GaAs* is strongly enhanced compared the polished sample. While the total photoluminescence quantum yield (η_{t})⁵⁹⁻⁶⁰ remains substantially unchanged after etching, the light absorption (Abs) nearly doubles (Table 1, see Experimental section for measurement details). The increase of light absorption, therefore, largely accounts for the twofold enhancement of integrated emission intensity seen in Figure 4. Interestingly, in the etched sample, the efficiency of the CV transition (η_{CV}) decreases by a 20%, while the efficiency of the IDS transition (η_{IDS}) is 2.5 times more efficient, yet the total quantum yield remains unaltered. This indicates that, upon absorption, a higher percentage of photoexcitations in *black GaAs* contribute to radiative intragap surface defect state transitions than to bulk interband recombination.

Conclusions

In conclusion, we demonstrated a new metal-assisted chemical etching process to create nearly perfect antireflection micro-structured GaAs surfaces in the visible and near-infrared spectral regions (*black*

GaAs). This solution-based process relies on a crystal plane dependent etch rate, which slows down at monoatomic gallium $\langle 111 \rangle$ and $\langle 311 \rangle$ crystallographic orientations regardless of the planes exposed to the etchant. Therefore, etching of the (100) or (111)B surfaces generates highly sloped microfacets which induce efficient light scattering and geometrical light trapping within the semiconductor surface, resulting in up to twofold enhancement of light absorption. We have shown that, on average, the antireflective properties of *black GaAs* are 2 to 10 times better than *black Si*, in which the reduction of surface reflectivity is induced by a refractive index matched surface nanowire layer, rather than by geometrical light trapping. As a result of increased absorption, the intensity of photoluminescence emitted by *black GaAs* doubles without affecting the external quantum efficiency, even though interband radiative recombination is reduced in favour of intragap surface defect state transitions. Given its simplicity and scalability, we believe that this method provides a viable way to increase the absorption of III-V semiconductors by microstructuring, and could be readily implemented into the production workflow of solar cells and photodetectors to increase their efficiency.

ASSOCIATED CONTENT

Supporting Information. Metal Assisted Chemical Etching (MACE) process. Electrodeless deposition of gold nanoparticles. MACE of (100) and (211) GaAs crystalline planes. Slow etching rate planes. Non-catalyzed etching of GaAs, Black Silicon reference; Antireflective properties, Diffuse reflectance measurements of polished and etched GaAs.

AUTHOR INFORMATION

Corresponding Author

* E-mail: csoci@ntu.edu.sg

Author Contributions

The manuscript was written through contributions of all authors.

ACKNOWLEDGMENTS

Research was supported by the Ministry of Education (MOE2011-T3-1-005, MOE2016-T2-1-052 and MOE2013-T2-1-044) and by the National Research Foundation (NRF-CREATE Singapore-Berkeley Research Initiative for Sustainable Energy, SinBeRISE) of Singapore. We also acknowledge support from the European Commission H2020 programme for the ETN SYNCHRONICS funded under grant agreement 643238. FC is a Royal Society Wolfson Foundation Research Merit Award.

1
2
3
4
5
6
7
8
9
10
11
12
13
14
15
16
17
18
19
20
21
22
23
24
25
26
27
28
29
30
31
32
33
34
35
36
37
38
39
40
41
42
43
44
45
46
47
48
49
50
51
52
53
54
55
56
57
58
59
60

REFERENCES

- 1
2
3 (1) Savin, H.; Repo, P.; von Gastrow, G.; Ortega, P.; Calle, E.; Garín, M.; Alcubilla, R. Black Silicon
4 Solar Cells with Interdigitated Back-Contacts Achieve 22.1% Efficiency. *Nat. Nanotechnol.* **2015**,
5 *10* (7), 624-628.
- 6
7 (2) Otto, M.; Algasinger, M.; Branz, H.; Gesemann, B.; Gimpel, T.; Füchsel, K.; Käsebier, T.;
8 Kontermann, S.; Koynov, S.; Li, X.; Naumann, V.; Oh, J.; Sprafke, A. N.; Ziegler, J.; Zilk, M.;
9 Wehrspohn, R. B. Black Silicon Photovoltaics. *Adv. Opt. Mater.* **2015**, *3* (2), 147-164.
- 10
11 (3) Tang, Z.; Tress, W.; Inganäs, O. Light Trapping in Thin Film Organic Solar Cells. *Mater. Today*
12 **2014**, *17* (8), 389-396.
- 13
14 (4) Lin, S.-H.; Su, Y.-H.; Cho, H.-W.; Kung, P.-Y.; Liao, W.-P.; Wu, J.-J. Nanophotonic Perovskite
15 Solar Cell Architecture with a Three-Dimensional TiO₂ Nanodendrite Scaffold for Light Trapping
16 and Electron Collection. *J. Mater. Chem. A* **2016**, *4* (3), 1119-1125.
- 17
18 (5) Du, Q. G.; Shen, G.; John, S. Light-Trapping in Perovskite Solar Cells. *AIP Advances* **2016**, *6* (6),
19 065002.
- 20
21 (6) Garnett, E.; Yang, P. Light Trapping in Silicon Nanowire Solar Cells. *Nano Lett.* **2010**, *10* (3),
22 1082-1087.
- 23
24 (7) Da, Y.; Xuan, Y.; Li, Q. From Light Trapping to Solar Energy Utilization: A Novel Photovoltaic-
25 Thermoelectric Hybrid System to Fully Utilize Solar Spectrum. *Energy* **2016**, *95*, 200-210.
- 26
27 (8) Brongersma, M. L.; Cui, Y.; Fan, S. Light Management for Photovoltaics Using High-Index
28 Nanostructures. *Nat. Mater.* **2014**, *13* (5), 451-460.
- 29
30 (9) Leung, S.-F.; Zhang, Q.; Xiu, F.; Yu, D.; Ho, J. C.; Li, D.; Fan, Z. Light management with
31 nanostructures for optoelectronic devices. *J. Phys. Chem. Lett.* **2014**, *5* (8), 1479-1495.
- 32
33 (10) Lova, P.; Soci, C. Nanoimprint Lithography: Toward Polymer Photonic Crystals. In *Organic and*
34 *hybrid photonic crystals*; Comoretto, D., Ed.; Springer: Cham, 2015; Chapter 187-212, p 493.
- 35
36 (11) Lova, P.; Cortecchia, D.; S. Krishnamoorthy, H. N.; Giusto, P.; Bastianini, C.; Bruno, A.;
37 Comoretto, D.; Soci, C. Engineering the Emission of Broadband 2D Perovskites by Polymer
38 Distributed Bragg Reflectors. *ACS Photonics* **2018**, *5* (3), 867-874.
- 39
40 (12) Miller, O. D.; Yablonovitch, E.; Kurtz, S. R. Strong Internal and External Luminescence As Solar
41 Cells Approach the Shockley-Queisser Limit. *IEEE J. Photovolt.* **2012**, *2* (3), 303-311.
- 42
43 (13) Li, X.; Bohn, P. W. Metal-Assisted Chemical Etching in HF/H₂O₂ Produces Porous Silicon. *Appl.*
44 *Phys. Lett.* **2000**, *77* (16), 2572-2574.
- 45
46 (14) Chartier, C.; Bastide, S.; Lévy-Clément, C. Metal-Assisted Chemical Etching of Silicon in HF-
47 H₂O₂. *Electrochim. Acta* **2008**, *53* (17), 5509-5516.
- 48
49 (15) Peng, K.; Lu, A.; Zhang, R.; Lee, S.-T. Motility of Metal Nanoparticles in Silicon And Induced
50 Anisotropic Silicon Etching. *Adv. Funct. Mater.* **2008**, *18* (19), 3026-3035.
- 51
52 (16) Zhang, M.-L.; Peng, K.-Q.; Fan, X.; Jie, J.-S.; Zhang, R.-Q.; Lee, S.-T.; Wong, N.-B. Preparation
53 of Large-Area Uniform Silicon Nanowires Arrays Through Metal-Assisted Chemical Etching. *J.*
54 *Phys. Chem. B* **2008**, *112* (12), 4444-4450.
- 55
56 (17) Jansen, H. V.; Boer, M. J. d.; Unnikrishnan, S.; Louwerse, M. C.; Elwenspoek, M. C. Black
57 Silicon Method X: A Review on High Speed and Selective Plasma Etching of Silicon with Profile
58 Control: An In-Depth Comparison Between Bosch and Cryostat Drie Processes as a Roadmap to
59 Next Generation Equipment. *J. Micromech. Microeng.* **2009**, *19* (3), 033001.
- 60

- 1 (18) Srivastava, S. K.; Kumar, D.; Singh, P. K.; Kar, M.; Kumar, V.; Husain, M. Excellent
2 Antireflection Properties of Vertical Silicon Nanowire Arrays. *Sol. Energy Mater. Sol. Cells* **2010**,
3 *94* (9), 1506-1511.
- 4 (19) Huang, Z.; Geyer, N.; Werner, P.; de Boor, J.; Gosele, U. Metal-Assisted Chemical Etching of
5 Silicon: a Review. *Adv. Mater.* **2011**, *23* (2), 285-308.
- 6 (20) Agnieszka, K.; Seán, T. B. Metal-Assisted Chemical Etching Using Sputtered Gold: A Simple
7 Route to Black Silicon. *Sci. Technol. Adv. Mater.* **2011**, *12* (4), 045001.
- 8 (21) Smith, Z. R.; Smith, R. L.; Collins, S. D. Mechanism of Nanowire Formation in Metal Assisted
9 Chemical Etching. *Electrochim. Acta* **2013**, *92*, 139-147.
- 10 (22) Rezvani, S. J.; Pinto, N.; Boarino, L. Rapid Formation of Single Crystalline Ge Nanowires by
11 Anodic Metal Assisted Etching. *Cryst. Eng. Comm* **2016**, *18* (40), 7843-7848.
- 12 (23) Elwenspoek, M.; Lindberg, U.; Kok, H.; Smith, L. In *Wet Chemical Etching Mechanism of*
13 *Silicon*, Micro Electro Mechanical Systems, 1994, MEMS '94, Proceedings, IEEE Workshop on,
14 1994; 1994; pp 223-228.
- 15 (24) Baca, A. G.; Ashby, C. I. H., Fabrication of GaAs Devices. Institution of Engineering and
16 Technology, EMIS processing series Bodmin, UK, 2005.
- 17 (25) Unagami, T. Formation mechanism of porous silicon layer by anodization in HF solution. *J.*
18 *Electrochem. Soc.* **1980**, *127* (2), 476-483.
- 19 (26) Peng, K.; Xu, Y.; Wu, Y.; Yan, Y.; Lee, S.-T.; Zhu, J. Aligned Single-Crystalline Si Nanowire
20 Arrays for Photovoltaic Applications. *Small* **2005**, *1* (11), 1062-1067.
- 21 (27) Liu, K.; Qu, S.; Zhang, X.; Wang, Z. Anisotropic Characteristics and Morphological Control of
22 Silicon Nanowires Fabricated by Metal-Assisted Chemical Etching. *J Mater Sci* **2013**, *48* (4),
23 1755-1762.
- 24 (28) Song, Y.; Choi, K.; Jun, D.-H.; Oh, J. Nanostructured GaAs Solar Cells via Metal-Assisted
25 Chemical Etching of Emitter Layers. *Opt. Express* **2017**, *25* (20), 23862-23872.
- 26 (29) Fang, H.; Wu, Y.; Zhu, J. H. Silver Catalysis in the Fabrication of Silicon Nanowire Arrays.
27 *Nanotechnology* **2006**, *17* (3), 3768.
- 28 (30) Yae, S.; Kawamoto, Y.; Tanaka, H.; Fukumoro, N.; Matsuda, H. Formation of Porous Silicon by
29 Metal Particle Enhanced Chemical Etching in HF Solution and its Application for Efficient Solar
30 Cells. *Electrochem. Commun.* **2003**, *5* (8), 632.
- 31 (31) Asoh, H.; Imai, R.; Hashimoto, H. Au-Capped GaAs Nanopillar Arrays Fabricated by Metal-
32 Assisted Chemical Etching. *Nanoscale Res. Lett.* **2017**, *12* (1), 444.
- 33 (32) Cheung, H.-Y.; Lin, H.; Xiu, F.; Wang, F.; Yip, S.; Ho, J. C.; Wong, C.-Y. Mechanistic
34 Characteristics of Metal-Assisted Chemical Etching in GaAs. *J. Phys. Chem. C* **2014**, *118* (13),
35 6903-6908.
- 36 (33) Yasukawa, Y.; Asoh, H.; Ono, S. Morphological Control of Periodic GaAs Hole Arrays by Simple
37 Au-Mediated Wet Etching. *J. Electrochem. Soc.* **2012**, *159* (5), D328-D332.
- 38 (34) DeJarld, M.; Shin, J. C.; Chern, W.; Chanda, D.; Balasundaram, K.; Rogers, J. A.; Li, X.
39 Formation of High Aspect Ratio GaAs Nanostructures with Metal-Assisted Chemical Etching.
40 *Nano Lett.* **2011**, *11* (12), 5259-5263.
- 41 (35) Mohseni, P. K.; Kim, S. H.; Zhao, X.; Balasundaram, K.; Kim, J. D.; Pan, L.; Rogers, J. A.;
42 Coleman, J. J.; Li, X. GaAs Pillar Array-Based Light Emitting Diodes Fabricated by Metal-
43 Assisted Chemical Etching. *J. App. Phys.* **2013**, *114* (6), 064909-6.

- 1
2
3
4
5
6
7
8
9
10
11
12
13
14
15
16
17
18
19
20
21
22
23
24
25
26
27
28
29
30
31
32
33
34
35
36
37
38
39
40
41
42
43
44
45
46
47
48
49
50
51
52
53
54
55
56
57
58
59
60
- (36) Asoh, H.; Suzuki, Y.; Ono, S. Metal-Assisted Chemical Etching of GaAs Using Au Catalyst Deposited on The Backside Of A Substrate. *Electochim. Acta* **2015**, *183*, 8-14.
- (37) Lee, A. R.; Kim, J.; Choi, S.-H.; Shin, J. C. Formation of Three-Dimensional GaAs Microstructures by Combination of Wet and Metal-Assisted Chemical Etching. *Phys. Status Solidi RRL* **2014**, *8* (4), 345-348.
- (38) Ono, S.; Kotaka, S.; Asoh, H. Fabrication and Structure Modulation of High-Aspect-Ratio Porous GaAs Through Anisotropic Chemical Etching, Anodic Etching, and Anodic Oxidation. *Electochim. Acta* **2013**, *110*, 393-401.
- (39) Song, Y.; Oh, J. Fabrication of Three-Dimensional GaAs Antireflective Structures by Metal-Assisted Chemical Etching. *Sol. Energy Mater. Sol. Cells* **2016**, *144*, 159-164.
- (40) Cowley, A.; Steele, J. A.; Byrne, D.; Vijayaraghavan, R. K.; McNally, P. J. Fabrication and Characterisation of GaAs Nanopillars Using Nanosphere Lithography and Metal Assisted Chemical Etching. *RSC Adv.* **2016**, *6* (36), 30468-30473.
- (41) Kong, L.; Song, Y.; Kim, J. D.; Yu, L.; Wasserman, D.; Chim, W. K.; Chiam, S. Y.; Li, X. Damage-Free Smooth-Sidewall InGaAs Nanopillar Array by Metal-Assisted Chemical Etching. *ACS Nano* **2017**, *11* (10), 10193-10205.
- (42) Glinsner, T.; Kreindl, G. *Lithography*, InTech: 2010; p 656.
- (43) Peng, K.; Zhang, M.; Lu, A.; Wong, N.-B.; Zhang, R.; Lee, S.-T. Ordered Silicon Nanowire Arrays via Nanosphere Lithography and Metal-Induced Etching. *App. Phys. Lett.* **2007**, *90* (16), 163123-3.
- (44) Radiative Transitions Induced In Gallium Arsenide by Modest Heat Treatment. *J. Appl. Phys.* **1980**, *51* (1), 619-624.
- (45) Im, K.; Kang, J.-H.; Park, Q. H. Universal Impedance Matching and The Perfect Transmission of White Light. *Nat. Photonics* **2018**, *12* (3), 143-149.
- (46) Momma, K.; Izumi, F. VESTA 3 for Three-Dimensional Visualization of Crystal, Volumetric And Morphology Data. *J. Appl. Crystallogr.* **2011**, *44* (6), 1272-1276.
- (47) <http://www.crystallography.net/result.php> retrieved on 21 May 2018.
- (48) de Mello, J. C.; Wittmann, H. F.; Friend, R. H. An Improved Experimental Determination of External Photoluminescence Quantum Efficiency. *Adv. Mater.* **1997**, *9* (3), 230-232.
- (49) Manfredi, G.; Lova, P.; Di Stasio, F.; Krahn, R.; Comoretto, D. Directional Fluorescence Spectral Narrowing in All-Polymer Microcavities Doped with CdSe/CdS Dot-in-Rod Nanocrystals. *ACS Photonics* **2017**, *4* (7), 1761-1769.
- (50) Lova, P.; Grande, V.; Manfredi, G.; Patrin, M.; Herbst, S.; Würthner, F.; Comoretto, D. All-Polymer Photonic Microcavities Doped with Perylene Bisimide J-Aggregates. *Adv. Opt. Mater.* **2017**, *5* (21), 1700523.
- (51) MacFadyen, D. N. On the Preferential Etching of GaAs by $\text{H}_2\text{SO}_4 \square \text{H}_2\text{O}_2 \square \text{H}_2\text{O}$. *J. Electrochem. Soc.* **1983**, *130* (9), 1934-1941.
- (52) Mikhael, B.; Elise, B.; Xavier, M.; Sebastian, S.; Johann, M.; Laetitia, P. New Silicon Architectures by Gold-Assisted Chemical Etching. *ACS Appl. Mater. Interfaces* **2011**, *3* (10), 3866-3873.
- (53) Bienaime, A.; Elie-Caille, C.; Leblois, T. Micro Structuration of GaAs Surface by Wet Etching: Towards a Specific Surface Behavior. *J. Nanosci. Nanotechnol.* **2012**, *12* (8), 6855-6863.

- 1 (54) Song, Y.; Oh, J. Thermally Driven Metal-Assisted Chemical Etching of GaAs with In-Position
2 and Out-Of-Position Catalyst. *J. Mater. Chem. A* **2014**, *2* (48), 20481-20485.
- 3 (55) Sailor, M. J. *Porous Silicon in Practice: Preparation, Characterization and Applications*, John
4 Wiley & Sons: 2012.
- 5 (56) Ky, N. H.; Reinhart, F. K. Amphoteric Native Defect Reactions in Si-Doped GaAs. *J. Appl. Phys.*
6 **1998**, *83* (2), 718-724.
- 7 (57) Ha, Y.-K.; Lee, C.; Kim, J.-E.; Park, H. Y.; Kim, S.; Lim, H.; Kim, B.-C.; Lee, H.-C. Defect
8 Luminescence in Heavily Si-Doped n-and p-Type GaAs. *J. Korean Phys. Soc.* **2000**, *36* (1), 42-
9 48.
- 10 (58) Sabataityt, J.; Šimkien, I.; Bendorius, R. A.; Grigoras, K.; Jasutis, V.; Pačebutas, V.; Tvardauskas,
11 H.; Naudžius, K. Morphology and Strongly Enhanced Photoluminescence of Porous GaAs Layers
12 Made by Anodic Etching. *Mater. Sci. Eng., Proc. Conf.* **2002**, *19* (1–2), 155-159.
- 13 (59) Takao, N.; Kyo-ichiro, F.; Taiji, O. Improvement of Quantum Efficiency in Gallium Arsenide
14 Electroluminescent Diodes. *Jpn. J. Appl. Phys.* **1967**, *6* (6), 665.
- 15 (60) Nelson, R. J.; Sobers, R. G. Minority Carrier Lifetimes and Internal Quantum Efficiency of
16 Surface-Free GaAs. *J. Appl. Phys.* **1978**, *49* (12), 6103-6108.
-
- 17
18
19
20
21
22
23
24
25
26
27
28
29
30
31
32
33
34
35
36
37
38
39
40
41
42
43
44
45
46
47
48
49
50
51
52
53
54
55
56
57
58
59
60

For Table of Contents only

Table of Contents artwork

